Geophysical Research Letters

RESEARCH LETTER
10.1029/2020GL088439

Key Points:
- Controlled CO_2-brine flow-through test with geophysical monitoring in fractured sandstone
- *P* wave velocity provides more reliable information about CO_2 content than shear wave anisotropy
- Elastic properties behave differently during CO_2 storage injection (drainage) and post injection (imbibition) stages

Supporting Information:
- Supporting Information S1

Correspondence to:
I. H. Falcon-Suarez,
isfalc@noc.ac.uk

Citation:
Falcon-Suarez, I. H., Papageorgiou, G., Jin, Z., Muñoz-Ibáñez, A., Chapman, M., & Best, A. I. (2020). CO_2-brine substitution effects on ultrasonic wave propagation through sandstone with oblique fractures. *Geophysical Research Letters*, *47*, e2020GL088439. https://doi.org/10.1029/2020GL088439

Received 16 APR 2020
Accepted 23 JUL 2020
Accepted article online 29 JUL 2020

Author Contributions:
Conceptualization: Ismael Himar Falcon-Suarez, Giorgos Papageorgiou
Data curation: Ismael Himar Falcon-Suarez, Andrea Muñoz-Ibáñez
Formal analysis: Giorgos Papageorgiou, Zhaoyu Jin
Funding acquisition: Ismael Himar Falcon-Suarez
Investigation: Zhaoyu Jin
Methodology: Ismael Himar Falcon-Suarez
Resources: Ismael Himar Falcon-Suarez, Mark Chapman, Angus I. Best
Supervision: Ismael Himar Falcon-Suarez, Giorgos Papageorgiou, Mark Chapman
Validation: Ismael Himar Falcon-Suarez, Giorgos Papageorgiou
(continued)

CO_2-Brine Substitution Effects on Ultrasonic Wave Propagation Through Sandstone With Oblique Fractures

Ismael Himar Falcon-Suarez[1], Giorgos Papageorgiou[2,3], Zhaoyu Jin[2], Andrea Muñoz-Ibáñez[4], Mark Chapman[2], and Angus I. Best[1]

[1]National Oceanography Centre, University of Southampton Waterfront Campus, Southampton, UK, [2]School of Geosciences, University of Edinburgh, Grant Institute, Edinburgh, UK, [3]Institute of Geoscience and Petroleum, NTNU, Trondheim, Norway, [4]School of Civil Engineering, University of A Coruña, A Coruña, Spain

Abstract Seismic monitoring of injected CO_2 plumes in fractured storage reservoirs relies on accurate knowledge of the physical mechanisms governing elastic wave propagation, as described by appropriate, validated rock physics models. We measured laboratory ultrasonic velocity and attenuation of *P* and *S* waves, and electrical resistivity, of a synthetic fractured sandstone with obliquely aligned (penny-shaped) fractures, undergoing a brine-CO_2 flow-through test at simulated reservoir pressure and temperature. Our results show systematic differences in the dependence of velocity and attenuation on fluid saturation between imbibition and drainage episodes, which we attribute to uniform and patchy fluid distributions, respectively, and the relative permeability of CO_2 and brine in the rock. This behavior is consistent with predictions from a multifluid rock physics model, facilitating the identification of the dispersive mechanisms associated with wave-induced fluid flow in fractured systems at seismic scales.

1. Introduction

From the microscopic scale to large faulting systems, cracks are present in almost every rock formation found in the Earth's crust. Anisotropic and potentially frequency-dependent wave propagation are key geophysical signatures describing cracked rocks. Such properties are crucial to assess the suitability of hydrocarbon reservoirs and saline aquifers for geological carbon storage (GCS) (Chiaramonte et al., 2015; Iding & Ringrose, 2010).

Previous studies have analyzed a number of factors affecting the brine-CO_2 saturation dependence in saline sandstone reservoirs—the most suitable geological context for GCS (Michael et al., 2010). These factors include the distinction between pore pressure and pore fluid distribution effects (Falcon-Suarez et al., 2016, 2017, 2018), the frequency dependence of elastic wave properties and the methodology to upscale information collected in laboratory (Lei & Xue, 2009; Mikhaltsevitch et al., 2014; Nakagawa et al., 2013), or the effect of mineralogical changes in the elastic and transport properties of the rock (Canal et al., 2013; Hangx et al., 2010, 2015; Vialle et al., 2014; Vialle & Vanorio, 2011). However, most of these studies are restricted to nonfractured rocks (Nooraiepour et al., 2018), although the nucleation and reactivation of fractures endanger safe GCS (Rutqvist, 2012; Velcin et al., 2020).

The distribution of different pore fluids is largely conditioned by reservoir heterogeneities, wettability (Al-Khdheeawi et al., 2017), and saturation history (Knight & Nolen-Hoeksema, 1990). To address the uncertainties associated with CO_2-brine partially saturated fractured rocks, we need to conduct controlled experiments on samples with well-defined physical and structural properties (e.g., Amalokwu et al., 2016; Rathore et al., 1995; Tillotson et al., 2011), to generate data sets to help constrain robust rock physics models. However, fluid-dependent phenomena dominating in laboratory observations such as frequency-dependent behavior or fluid distribution in the pore space are rarely examined in conjunction with their intrinsic anisotropy (Amalokwu et al., 2014; Murphy, 1984).

Few rock physics theories incorporate the subtleties associated with such partially saturated cracked rocks holistically. Recently, Papageorgiou and Chapman (2017) have suggested a theory that combines uniform/patchy fluid distribution (Dutta & Odé, 1979; White, 1975) and squirt flow (Chapman, 2003;

Visualization: Ismael Himar Falcon-Suarez
Writing - original draft: Ismael Himar Falcon-Suarez, Giorgos Papageorgiou
Writing – review & editing: Andrea Muñoz-Ibáñez, Angus I. Best

Dvorkin et al., 1995) phenomena for partially saturated isotropic rocks. Later, Jin et al. (2018) extended their work to incorporate mesoscopic flow that occurs between fractures and the pore space for anisotropic rocks. The model of Jin et al. (2018) is therefore appropriate to describe frequency-dependent wave velocities of partially saturated, cracked samples. If properly calibrated, this model also could be used to describe seismic velocities obtained during and after CO_2 injection in fractured GCS reservoirs.

Here, we present a brine-CO_2 partial saturation experiment in cracked sandstone with a well-defined fracture network (cracks aligned at oblique angle), under realistic geological conditions of confining (40 MPa) and pore (10 MPa) pressure. During the test, we measured ultrasonic *P* and two orthogonal *S* wave velocities and attenuations, together with electrical resistivity that we used to determine the evolution of the degree of CO_2 saturation (up to ~60%, including drainage and imbibition saturation paths). We simultaneously fit ultrasonic velocities to constrain the rock physics model of Jin et al. (2018), which explains the observed anisotropic and dispersive properties, and variation with partial saturation, as well as a counterintuitive increase of the velocity despite the decrease of stiff fluid. The transport and mechanical results are assessed in Muñoz-Ibáñez et al. (2019).

2. Experimental Procedure

We used a ~2-cm length, ~5-cm diameter synthetic sandstone core plug, containing fractures aligned at 45° from its axis. The sample was manufactured using a mixture of sand, kaolinite, and sodium silica gel (Falcon-Suarez et al., 2019), but with a predetermined number of 2-mm diameter (δ), 0.2-mm thickness (τ) aluminum discs (Amalokwu et al., 2015; Tillotson et al., 2012). Once baked, the sample was immersed in an acidic bath to remove the aluminum discs, resulting in a silica-cemented sandstone with 45° aligned penny-shaped cracks. The fracture density ($\varepsilon_f = 0.0298 \pm 0.0077$) and an average fracture aspect ratio ($\tau/\delta = 0.088 \pm 0.001$) were obtained from X-ray CT scan image processing (Amalokwu et al., 2015), which leads to a porosity fraction attributed to fractures of ~10% (Muñoz-Ibáñez et al., 2019).

A set of 90° biaxial 350-ohm electrical strain gauges was epoxy glued on the lateral side wall of the sample to measure axial and radial strains during the test. Porosity (ϕ) by He pycnometry and permeability to nitrogen (k_{gas}) were determined under minimal confining stress (~0.5 MPa) before ($\phi_0 = 27.3 \pm 0.6\%$; $k_{gas,0} = 5.5 \pm 3.13$ mD) and after ($\phi_f = 29.6 \pm 0.7\%$; $k_{gas,f} = 12.1 \pm 3.24$ mD) the test.

The sample was subjected to steady-state brine-CO_2 flow-through (BCFT), using the experimental rig for CO_2 storage multiflow tests described in Falcon-Suarez et al. (2017). The rig implements sensors for measuring, simultaneously, electrical resistivity and ultrasonic waves (velocity and attenuation) using the pulse echo technique (Amalokwu, 2016; Best, 1992; McCann & Sothcott, 1992). Here, we used a sensor that incorporates *P* and *S* wave transducers in one platen, and a single *S* wave transducer in the other (all transmitting 400- to 1,000-kHz broadband acoustic pulses). For these transducers, the velocity precision is ±0.1% with an accuracy of ±0.3% (95% confidence), while attenuation accuracy is ±0.2 dB/cm (Best, 1992). The *S* wave transducer polarizations were aligned parallel and perpendicular to the fracture strike, measuring oblique S_1 (fast) and S_2 (slow) wave velocity and attenuation, respectively, for estimations of the shear wave anisotropy (expressed as $(n_{S1} - n_{S2})/n_{S1}$, for a given *S* wave attribute n).

The BCFT test was conducted under constant hydrostatic confining ($P_c = 40$ MPa) and pore ($P_p = 10$ MPa) pressure, at room temperature (20°C), using 3.5% NaCl synthetic brine and liquid CO_2, and covered drainage and imbibition episodes. An overpressure limit of 2 MPa was imposed (Muñoz-Ibáñez et al., 2019), which prevents rock mechanical damage (fracture propagation) at the simulated conditions (Velcin et al., 2020). The total flow ($Q = Q_w + Q_{CO2}$) was initially regulated in each episode ($Q < 0.5$ cm^3 min^{-1}), and the CO_2 fractional flow ($X_{CO2} = Q_{CO2}/Q$) increased in 0.2 units episodes during the drainage part of the test. After the last drainage episode, the BCFT test concluded with a 100% brine flow-through to force the natural imbibition process that occurs in saline aquifers after ceasing the CO_2 injection (Gaus, 2010).

During the test, axial and radial strains were measured continuously (every second), while ultrasonic *P* and $S_{1,2}$ wave velocities (V_P, $V_{S1,2}$) and attenuations (inverse quality factors Q_P^{-1}, $Q_{S1,2}^{-1}$), and resistivity were acquired, at least, every 0.5 times the sample pore volume (PV ~ 10.46 cm^3) of flow-through. Then, using Archie's (1942) first and second laws, the bulk resistivity of porous media partially saturated with brine and CO_2 was transformed into degree of brine saturation (Carrigan et al., 2013; Falcon-Suarez et al., 2016,

2017, 2018; Muñoz-Ibáñez et al., 2019; Nakatsuka et al., 2010). For resistivity, the error increases from <1% up to 5% with resistivity and sample anisotropy (North et al., 2013). The upper value leads to a saturation uncertainty of ±5%, when converting resistivity into degree of saturation using Archie's approach with a saturation exponent $n = 2$, usually adopted for sandstones (Mavko et al., 2009). However, the dual porosity of our sample influences the rock wettability and the saturation history (Muñoz-Ibáñez et al., 2019). In turn, n might become variable for a given resistivity-saturation relationship, invalidating the use of Archie's law (Suman & Knight, 1997; Zhou & Stenby, 1997). To account for this, we propagate saturation error derived from ±10% variations in n, which covers the deviation from drainage to imbibition in nonuniform pore size distribution in water-wet samples (Suman & Knight, 1997).

After the BCFT test, the sample was cleaned with deionized water and then dried, before being saturated with CO_2 at the test conditions to collect the corresponding ultrasonic properties. Further information about the testing methodology in Falcon-Suarez et al. (2017), Muñoz-Ibáñez et al. (2019) and as supporting information in the online version of this manuscript.

3. Results

3.1. Ultrasonic Waves

The pulse-echo method used in this study (Winkler & Plona, 1982) provides accurate measurements of ultrasonic velocities and attenuation (Amalokwu, 2016; Best, 1992; Best et al., 2007; Tillotson et al., 2011, 2012). Figure 1a shows energy dissipation related to multiple arrivals for both the *P* and *S* wave signals between top and base reflection peaks (framed within the data-processing windows W1 and W2, respectively). The energy dissipation is independent of the partial saturation for S_1 and S_2, which trends are almost identical under different partial CO_2 saturations (S_{CO2}), while multiple internal reflections distort the signal after the first pulse. *P* wave also evidences scattering arrivals in the time between the top and base reflections, but varies with the saturation state, which magnifies the overall energy dissipation, as calculated from the reduction in amplitude of the base reflection relative to the top reflection.

The horizontal and vertical cross-sections of the fractures (Figure 1b) show local fracture propagation that in some cases can exceed original fracture length (e.g., Y3). This fracture elongation is preferentially inducing energy dissipation for *S* waves, which the wavelength (3 mm) is closer to the fracture length (2 mm) than that of *P* waves (5 mm). Therefore, the attenuation data shown in Figure 2 have to be understood in qualitative terms, with Q_P^{-1} showing significant changes between drainage and imbibition paths, while the Q_{S1}^{-1} and Q_{S2}^{-1} are largely affected by scattering with no significant changes (i.e., variations lie within the experimental error).

3.2. BCFT Test

The brine-CO_2 flow-through (BCFT) test lasted ~75 hr, resulting in a total fluid throughput of ~63 PV. Figure 2 shows the ultrasonic properties (V_P, $V_{S1,2}$ and Q_P^{-1}, $Q_{S1,2}^{-1}$; all the results at 600 kHz obtained from Fourier analysis of the broadband signals), plotted together with the electrical resistivity and volumetric strains measured during the BCFT test.

The transition from the first brine: CO_2 fractional flow episode ($X_{CO2} = 0$) to the second ($X_{CO2} = 0.2$) marks the arrival of the free CO_2 phase in the rock (PV ~3.6), and the resistivity increases progressively with the volume of CO_2 passing through the rock. The CO_2 arrival leads to a sharp increase of V_P (~1.5%) and Q_p^{-1} (~50%), followed by a progressive decrease of V_P with the increasing CO_2 content and the opposite for Q_P^{-1}. The two orthogonal components of the shear wave show similar trends in both the velocities (V_{S1}, V_{S2}) and the attenuations (Q_{S1}^{-1}, Q_{S2}^{-1}), with relative differences of ~6% between V_{S1} and V_{S2} and throughout the BCFT test. V_{S1} and V_{S2} drop during $X_{CO2} = 0.2$, followed by a soft increasing trend thereafter. Similarly, Q_{S1}^{-1} and Q_{S2}^{-1} progressively increase during drainage and drop to approximately the original values during the forced imbibition episode (X_{CO2} = R-0). However, this trend is inconclusive as it occurs within the experimental uncertainty.

The imbibition (R-0) started with a single brine pulse (~0.5 PV at 42.8 PV; BP in Figure 2), with continuous monitoring of the geophysical properties of the sample. Then, continuous brine flow through the sample was progressively replacing the CO_2 from the pore space, as inferred from the resistivity drop (down to ~24%

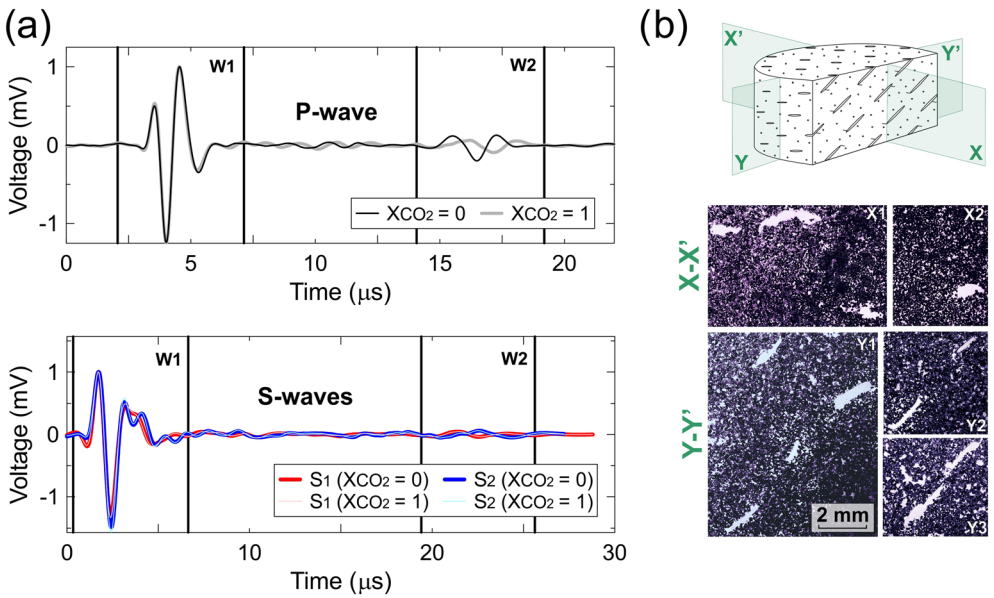

Figure 1. P and $S_{1,2}$ wave signals (a) at the saturation states corresponding to fractional flow episodes of pure brine ($X_{CO2} = 0$) and CO_2 ($X_{CO2} = 1$). W1 and W2 indicate the time windows used for the Fourier analysis (Best, 1992). (b) Thin section analysis from two (mutually orthogonal) slides prepared after the BCFT test. From original images, color channel filtering was applied to emphasize porous (bright) with respect to grains (dark) areas.

above the original brine-saturated conditions). The imbibition affected P and S wave properties differently: V_P increased and Q_P^{-1} decreased, both up to ~2% below and above the original brine-saturated values, respectively, while $V_{S1,2}$ and $Q_{S1,2}^{-1}$ fully recovered by the end of the imbibition. Yin et al. (1992) also found that the attenuation depends not only on the degree of saturation and the frequency of the measurements but also on the saturation history. They reported ~7% shift on the degree of saturation for the attenuation peak from drainage to imbibition paths at sonic frequencies (~1,500 Hz). In our case, this shift reaches up to 30% for Q_P^{-1} (Figure 2), because of the interplay of the scattering on heterogeneities (crack-induced internal reflections) and energy dispersive mechanisms related to partial fluid flow in porous media. This render the attenuation measurements unreliable as quantitative indicators of the changing physical properties of the sample due to pore fluid substitution.

The sample evidences mechanical deformation (inflation) after $X_{CO2} > 0.5$, which stabilizes during imbibition. This minor inflation (~0.12%) is within the porosity fraction commonly attributed to microcracks (0.7%; Fortin et al., 2007). Thus, it could be related to microcracks reopening due to differential pressure ($P_{diff} = P_c - P_p$) drop during the experiment associated with the increase of inlet-to-outlet P_p gradients with the increasing X_{CO2} (Muñoz-Ibáñez et al., 2019).

4. Insights From Data Analysis

Theories for wave propagation through partially saturated rocks emphasize two dominant dispersive mechanisms taking place when wave propagation induces local and mesoscale fluid flow: squirt flow (Chapman, 2003; Dvorkin et al., 1995) and patchy saturation (Dutta & Odé, 1979; White, 1975) effects. While the diffusive character of Biot flow (Biot, 1956) is significant in unconsolidated sediments, in consolidated rocks, the predicted dispersion is much smaller and occurs at much higher frequencies than the experimental frequency. We therefore focus on the first two: squirt flow and patchy saturation.

Papageorgiou and Chapman (2017) combined these two effects into a single theory. Later, Jin et al. (2018) extended their theory to include anisotropic effects due to fractures, showing that the moduli of a fractured, partially saturated rock can be interpreted as two coupled standard linear solid (SLS) models (Mavko et al., 2009). These two SLS models have relaxation frequencies linked by the scale ratio of the fracture size to the pore/microcrack size. For a rock with aligned fractures, the SLS with lower relaxation frequency

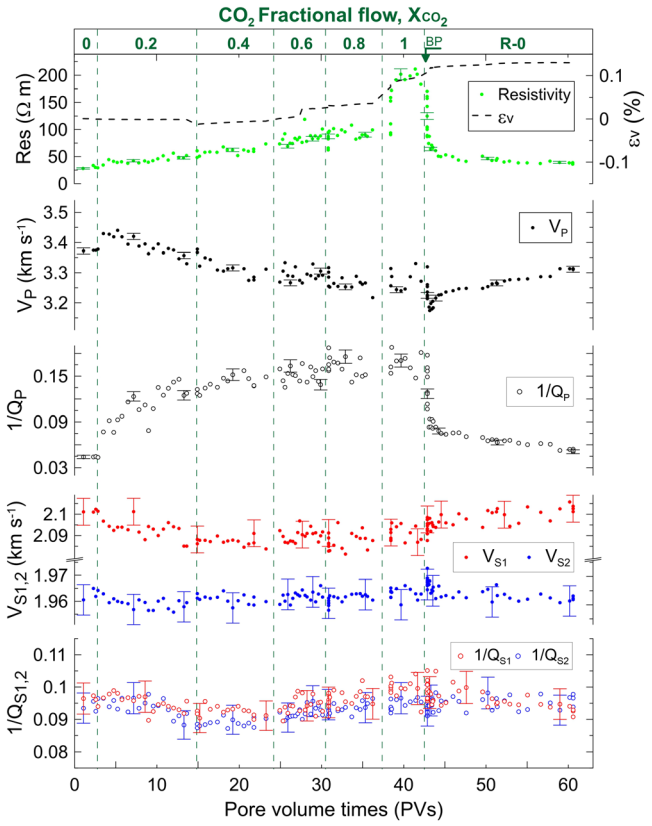

Figure 2. Brine-CO_2 flow-through test in fracture sandstone. *P* and $S_{1,2}$ wave velocities (V_P, $V_{S1,2}$), attenuations (Q_P^{-1}, $Q_{S1,2}^{-1}$) and electrical resistivity, together with volumetric strains for six brine: CO_2 flow rates drainage episodes (X_{CO2} = 0 to 1) and the forced imbibition (X_{CO2} = R-0; BP denotes the initial imbibition brine pulse; see text). The ultrasonic properties were measured at a single frequency of 600 kHz (pulse-echo technique), obtained from the Fourier analysis of broad band signals. Error bars displayed every 10 measurements.

corresponds to an anisotropic mechanism that induces dispersion in the fracture normal direction only, whereas the SLS with higher relaxation frequency is isotropic.

In partial saturation, both the combined squirt-patch effect and the effective fluid moduli impact the two SLS relaxation frequencies (Brie et al., 1995; Papageorgiou & Chapman, 2017). The relaxation frequencies depend on relative permeability and a patch parameter *q*, which lies between 1 at uniform saturation and the ratio of the fluid moduli at patchy saturation (Papageorgiou & Chapman, 2017). The magnitude of each SLS model induced dispersion is controlled by the fracture density (ε_f) and by microcrack density (ε_m), for the SLS with lower relaxation frequency and higher relaxation frequency, respectively.

To calculate the relaxation frequencies at partial saturation, we use the Brooks-Corey relative permeability model, suitable for explaining the two fluid phases' interaction in our sample (Muñoz-Ibáñez et al., 2019), and the fracture and microcrack densities $\varepsilon_f = 0.042$ and $\varepsilon_m = 0.02$. ε_f is derived from the design of synthetic fractures in the sample (Tillotson et al., 2012), while ε_m is arbitrarily adopted within the range of values observed in similar synthetic rocks (Papageorgiou et al., 2018). In the Supporting Information, we show how we derive the V_P, V_{S1}, V_{S2} of an effective medium with these properties. The increase in V_P at low saturation, together with the absence of fluid-dependent shear wave anisotropy, is consistent with the behavior of our model in the frequency regime, where the large fractures are effectively sealed but squirt flow dispersion is still observable isotropically. Current data prevent us from further constraining these frequencies, so we present modeling for a range of relaxation frequencies of the microcrack SLS relative to the experiment frequency, as well as saturation distribution scenarios for patchy and uniform saturated pores.

Figure 3 summarizes our modeling results, considering the relaxation frequency and fluid distribution scenarios (Figure 3a) and the model's predictions for V_P, V_S and shear wave anisotropy (Figures 3b–3d). For the fit, we perform a nonlinear Nelder-Mead minimization in two steps for each of the three relaxation frequencies ω_i. First, we deduce effective medium matrix parameters λ, μ at full water saturation; that is, we determine λ, μ given constant ε, ε_f, ω_i such that, when $S_w = 1$, $(V_{P(th)}(\lambda,\mu) - V_{P(ex)})^2 + (V_{S1(th)}(\lambda,\mu) - V_{S1(ex)})^2 + (V_{S2(th)}(\lambda,\mu) - V_{S2(ex)})^2$ is minimum (subscripts "th" and "ex" for theoretic and experimental, respectively). As a second step, we invert for the patch parameter at partial saturation for each of the imbibition/drainage stages; that is, given λ, μ, ε, ε_f, ω_i, we determine *q* such that $\sum_{S_j}\left(\left(V_{P(theor)}(q) - V_{P(exp)}\right)^2 + \left(V_{S1(theor)}(q) - V_{S1(exp)}\right)^2 + \left(V_{S2(theor)}(q) - V_{S2(exp)}\right)^2\right)$ is minimum, where S_j are the saturation steps for which we have data.

Despite the difference in fluids and incomplete saturation path, our V_P results are similar in form to the observations in Knight and Nolen-Hoeksema (1990), where velocities showed strong hysteresis with values consistently higher during drainage. Knight and Nolen-Hoeksema (1990) attribute this discrepancy to a difference in pore-fluid distribution under drainage (patchy saturation) and imbibition (uniform saturation), which is consistent with our observations. However, we note the lack of significant V_S hysteresis and the strong impact of the saturation distribution to the velocity dispersion in our work.

The absence of imbibition data with $S_w \geq 0.85$ prevents saturation history analysis at the high saturation regime and indicates a residual CO_2 trapping of ~15% at the experimental conditions. However, the

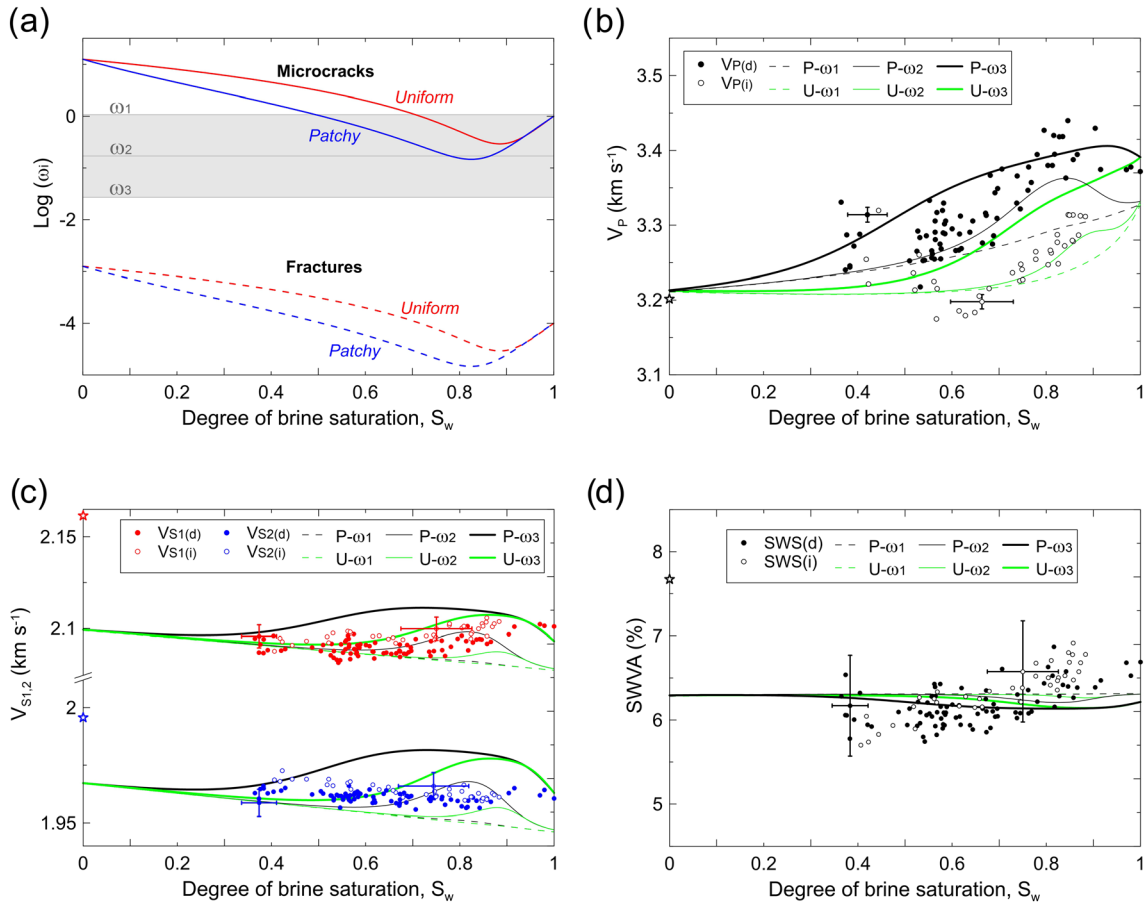

Figure 3. (a) Patchy and uniform models for microfractures and fractures frequency domains. Ultrasonic *P* and *S* wave velocities V_P (b), V_{S1} and V_{S2} (c), and *S* wave velocity anisotropy, SWVA $= (V_{S1} - V_{S2})/V_{S1} \times 100$ (d), versus degree of brine saturation (S_w). Two modeling scenarios for pore fluid distribution: uniformly (U, with patch parameter q = 1) and patchy (P, with q = 0.2), at frequencies $\omega_1 = 0.027$, $\omega_2 = 0.17$, and $\omega_3 = 1.0725$. Subscripts d and i refer to drainage and imbibition, respectively. The star symbol indicates the CO_2 saturation measurement (see text). Two single cross bars show horizontal and vertical errors for low and high S_w.

increase observed in porosity (~5%) and permeability (~45%) after the BCFT test might have occurred during drainage. Then, abnormally high values of $V_{S1,2}$ measured at full CO_2 saturation (marked by stars in Figure 3), together with the elevated $V_{S1,2}$ and reduced V_P values with respect to modeling along the imbibition path, indicate the reduction of the sample's density (i.e., porosity increase) affected its shear modulus minimally, in agreement with Delle Piane and Sarout (2016).

We also observe a striking increase in V_P at low CO_2 saturation (S_w ~ 0.9), despite the addition of softer fluid in the system. Given the similar density between the CO_2 and brine, this increase is attributed to an increase in the elastic modulus. This phenomenon is unusual but still identified in previously reported data for sandstones (Batzle et al., 2006), limestones (Cadoret et al., 1995), and shales (Szewczyk et al., 2018), with air and water as pore fluids under atmospheric pressure conditions. In our experiment, the viscosity and moduli of the two fluids differ by only one or two orders of magnitude within the experimental bandwidth, which magnifies the observed effect with respect to the previous observations. This increase is also present in the modeling predictions, and we have excluded CO_2 dissolution into water as a possible cause for this phenomenon as its impact would be of the order of <1%, much smaller than the observation. The reason for this increase lies in the complex interplay between partial fluid mobility and effective fluid modulus: a S_w range exists between 0.8 and 0.9 in which the dispersion from frequency-dependent effects overcompensates for the addition of the soft fluid, making the system stiffer at partial than at full saturation.

5. Discussion

The ultimate goal of our work is to understand the geophysical behavior of fractured reservoirs undergoing CO_2 injection and identify the mechanisms that can be used to effectively monitor GCS projects. We extend the work of Nooraiepour et al. (2018) in considering properties of distributions of fractures, which is closer to the equivalent medium concept required to scale to reservoir conditions. To date, data regarding partial saturation in fractured media are limited to controlled experiments at atmospheric conditions using water and air as nonwetting phase (e.g., Amalokwu, 2016). The air has higher compressibility, lower viscosity, and density 3 orders of magnitude lower than ours at the experimental conditions (i.e., liquid CO_2). Therefore, we expect to find discrepancies between our results and those found in the literature related to the nonwetting fluid properties.

The properties of the pore fluids and their mobility through the porous media complicate the distinction between pore fluid distribution and rock fabric in fractured media. Kong et al. (2017) remarked that the fracture-filling fluid can disguise *P* wave dispersion and attenuation effects due to fracture orientation, when its modulus is much smaller than that of the pore-filling fluid. Amalokwu et al. (2015) found that fractures obliquely oriented with respect to wave propagation can lead to *S* wave velocity anisotropy (SWVA) drop with increasing water saturation, because V_{S2} (sensitive to fluid compressibility reduction) decreases, while V_{S1}, considered independent of the pore fluid (Tillotson et al., 2012), remains constant. Conversely, our results show minor SWVA variation with the CO_2 content, within the bounds imposed by experimental error.

The distribution of the two fluids in our porous medium is conditioned by the wettability of the CO_2-brine-rock system, the pore geometry, and the saturation history (Cinar & Riaz, 2014; Krevor et al., 2015). Our experiment simulates different stages of CO_2 injection in fractured saline siliciclastic reservoirs, at realistic geological stress conditions. The test covers fluid substitution during CO_2 plume advance (drainage) and the natural aquifer recharge after ceasing the injection activities (imbibition) with a maximum CO_2 saturation ~0.6, in agreement with previous CO_2-water fluid substitution tests in sandstones (Burnside & Naylor, 2014). The low capillarity forces of the fractures with respect to the pores lead to preferential CO_2 fracture filling (Muñoz-Ibáñez et al., 2019), which magnifies the effect of drainage versus imbibition paths.

Our results indicate that *P* wave properties (V_P, $Q_P{}^{-1}$) are highly sensitive to the saturation history, while *S* waves show very little differences between drainage and imbibition saturation paths. This finding has important implications for CO_2 storage, since the information inferred from seismic surveys during the injection and post injection activities are significantly different; but this also applies for the differential monitoring of the front (drainage) and the trailing edge (imbibition) of the CO_2 plume. The degree of partial saturation in sandstones with fractures aligned at oblique angles might have some effect in the SWVA, in agreement with Amalokwu et al. (2016), but certainly insufficient to be used as a robust indicator of pore fluid distribution. This finding has direct application on the interpretation of *S* wave splitting data sets from gas and GCS reservoirs containing or developing fractures during production or injection activities.

The use of ultrasonic waves to explore fractured media is influenced by the characteristics of the fracture, such as fracture length (c), aperture, crack surface roughness, and the saturating fluid, as well as the wavelength (λ_w). If $c/\lambda_w < 1$, the porous medium appears homogeneous, while for $c/\lambda_w > 1$, heterogeneities begin to act as energy scattering fronts. In our rock sample, c is slightly lower than λ_w for both the *P* and *S* waves, which leads to some wave scattering in the recorded signals. In addition, regardless of how homogeneous the medium is, absolute scale also plays a part.

Here, we identify and analyze the mechanisms that are necessary to describe an effective medium that reproduces the dispersive behavior of the rock. The results from our controlled experiment suggest that fluid flow induces dispersive behavior at the pore and fracture scale (with a transition frequency that scales with effective mobility), which is sufficient to describe this fractured medium. Likewise, we observe that despite the single experimental frequency, dispersion varies across saturation consistently with our modeling strategy indicating that the dominant mechanisms—at least with respect to wave-induced fluid flow—have been taken into account in the effective medium. This interpretation is supported by Figure 3, where the counterintuitive features of the model are reproduced, such as the increase of compressional velocity at intermediate

saturation depending on drainage/imbibition paths, in conjunction with the relatively small dispersion in shear wave velocities.

Likewise, we anticipate that a fractured, partially saturated reservoir rock will exhibit dispersive behavior according to these mechanisms at the field scale. To make this fully predictive, we would need to calibrate the model with specific field velocity measurements and have a hydrological characterization of the reservoir formation. Our identification of these mechanisms offers a step toward overcoming the difficulty in distinguishing saturation effects from fluid distribution effects in fractured systems. This problem is dominant in the characterization and monitoring of CO_2 storage reservoirs where faults have been recognized (Chiaramonte et al., 2015; Iding & Ringrose, 2010).

6. Conclusions

In this work, we record experimental observation suggesting anisotropic rocks with aligned fractures have bulk and shear elastic behavior that depends on the saturation path (imbibition/drainage). During our high-pressure brine-CO_2 flow-through experiment on a synthetic sandstone, stiffening was observed for low (~10%) CO_2 saturation in the drainage phase, despite the apparent fluid softening. We found shear wave velocity anisotropy to be independent of saturation path and were unable to draw conclusions about its dependence on fluid content due to high uncertainties associated with the *S* wave measurements. Using recently published work, we were able to explain the dependence of the elastic constants on imbibition and drainage. We observe manifestations of different patchiness in the fluid distribution, with more uniform saturation during imbibition and patchy saturation during drainage, in accordance to previously published experiments performed on isotropic rocks. Using the same rock physics model, we were able to capture the increase in modulus observed during drainage as a result from a decrease in effective mobility due to relative permeability effects.

Data Availability Statement

Data presented in this study are available at the U.K. National Geoscience Data Centre (NGDC) repository (https://doi.org/10.5285/abc38c58-3a69-42ed-86ac-1502509bd88c).

Acknowledgments

We have received funding from the U.K.'s Natural Environment Research Council (grant NE/R013535/1 GASRIP and grant NE/N016041/1 CHIMNEY), the European Union's Horizon 2020 research and innovation programme (grant no. 654462 STEMM-CCS), the program PETROMAKS2 of the Research Council of Norway (RCN grant number: 267765), and the Xunta de Galicia and the European Union (European Social Fund—ESF). Zhaoyu Jin was supported by the Principal's Career Development PhD Scholarship and Edinburgh Global Research Scholarship from The University of Edinburgh. The experiment was conducted at the NOC Rock Physics Laboratory in Southampton. The authors thank Dr. Laurence North for his support in the laboratory with the geophysical measurements.

References

Al-Khdheeawi, E. A., Vialle, S., Barifcani, A., Sarmadivaleh, M., & Iglauer, S. (2017). Impact of reservoir wettability and heterogeneity on CO_2-plume migration and trapping capacity. *International Journal of Greenhouse Gas Control*, *58*, 142–158. https://doi.org/10.1016/j.ijggc.2017.01.012

Amalokwu, K. (2016). Saturation effects on frequency-dependent seismic anisotropy in fractured porous rocks, Doctoral thesis, 168 pp, University of Southampton.

Amalokwu, K., Best, A. I., & Chapman, M. (2016). Effects of aligned fractures on the response of velocity and attenuation ratios to water saturation variation: A laboratory study using synthetic sandstones. *Geophysical Prospecting*, *64*(4), 942–957. https://doi.org/10.1111/1365-2478.12378

Amalokwu, K., Best, A. I., Sothcott, J., Chapman, M., Minshull, T., & Li, X.-Y. (2014). Water saturation effects on elastic wave attenuation in porous rocks with aligned fractures. *Geophysical Journal International*, *197*(2), 943–947. https://doi.org/10.1093/gji/ggu076

Amalokwu, K., Chapman, M., Best, A. I., Sothcott, J., Minshull, T. A., & Li, X.-Y. (2015). Experimental observation of water saturation effects on shear wave splitting in synthetic rock with fractures aligned at oblique angles. *Geophysical Journal International*, *200*(1), 17–24. https://doi.org/10.1093/gji/ggu368

Archie, G. E. (1942). The electrical resistivity log as an aid in determining some reservoir characteristics, https://doi.org/10.2118/942054-G

Batzle, M. L., Han, D.-H., & Hofmann, R. (2006). Fluid mobility and frequency-dependent seismic velocity—Direct measurements. *Geophysics*, *71*(1), N1–N9. https://doi.org/10.1190/1.2159053

Best, A. I. (1992). The prediction of the reservoir properties of sedimentary rocks from seismic measurements, 393 pp, University of Reading.

Best, A. I., Sothcott, J., & McCann, C. (2007). A laboratory study of seismic velocity and attenuation anisotropy in near-surface sedimentary rocks. *Geophysical Prospecting*, *55*(5), 609–625. https://doi.org/10.1111/j.1365-2478.2007.00642.x

Biot, M. A. (1956). Theory of Propagation of Elastic Waves in a Fluid-Saturated Porous Solid. II. Higher Frequency Range. *The Journal of the Acoustical Society of America*, *28*(2), 179–191. https://doi.org/10.1121/1.1908241

Brie, A., Pampuri, F., Marsala, A. F., & Meazza, O. (1995). Shear sonic interpretation in gas-bearing sands, in SPE Annual Technical Conference and Exhibition, edited, p. 10, Society of Petroleum Engineers, Dallas, Texas.

Burnside, N. M., & Naylor, M. (2014). Review and implications of relative permeability of CO_2/brine systems and residual trapping of CO_2. *International Journal of Greenhouse Gas Control*, *23*, 1–11. http://doi.org/10.1016/j.ijggc.2014.01.013

Cadoret, T., Marion, D., & Zinszner, B. (1995). Influence of frequency and fluid distribution on elastic wave velocities in partially saturated limestones. *Journal of Geophysical Research*, *100*(B6), 9789–9803. https://doi.org/10.1029/95JB00757

Canal, J., Delgado, J., Falcón, I., Yang, Q., Juncosa, R., & Barrientos, V. (2013). Injection of CO_2-saturated water through a siliceous sandstone plug from the Hontomin test site (Spain): Experiment and modeling. *Environmental Science & Technology*, *47*(1), 159–167. http://doi.org/10.1021/es3012222

Carrigan, C. R., Yang, X., LaBrecque, D. J., Larsen, D., Freeman, D., Ramirez, A. L., et al. (2013). Electrical resistance tomographic monitoring of CO_2 movement in deep geologic reservoirs. *International Journal of Greenhouse Gas Control*, *18*, 401–408. http://doi.org/10.1016/j.ijggc.2013.04.016

Chapman, M. (2003). Frequency-dependent anisotropy due to meso-scale fractures in the presence of equant porosity. *Geophysical Prospecting*, *51*(5), 369–379. https://doi.org/10.1046/j.1365-2478.2003.00384.x

Chiaramonte, L., White, J. A., & Trainor-Guitton, W. (2015). Probabilistic geomechanical analysis of compartmentalization at the Snøhvit CO_2 sequestration project. *Journal of Geophysical Research: Solid Earth*, *120*, 1195–1209. https://doi.org/10.1002/2014JB011376

Cinar, Y., & Riaz, A. (2014). Carbon dioxide sequestration in saline formations: Part 2—Review of multiphase flow modeling. *Journal of Petroleum Science and Engineering*, *124*, 381–398. https://doi.org/10.1016/j.petrol.2014.07.023

Delle Piane, C., & Sarout, J. (2016). Effects of water and supercritical CO_2 on the mechanical and elastic properties of Berea sandstone. *International Journal of Greenhouse Gas Control*, *55*, 209–220. http://doi.org/10.1016/j.ijggc.2016.06.001

Dutta, N. C., & Odé, H. (1979). Attenuation and dispersion of compressional waves in fluid-filled porous rocks with partial gas saturation (White model)—Part I: Biot theory. *Geophysics*, *44*(11), 1777–1788. https://doi.org/10.1190/1.1440938

Dvorkin, J., Mavko, G., & Nur, A. (1995). Squirt flow in fully saturated rocks. *Geophysics*, *60*(1), 97–107. https://doi.org/10.1190/1.1443767

Falcon-Suarez, I., Marín-Moreno, H., Browning, F., Lichtschlag, A., Robert, K., North, L. J., & Best, A. I. (2017). Experimental assessment of pore fluid distribution and geomechanical changes in saline sandstone reservoirs during and after CO_2 injection. *International Journal of Greenhouse Gas Control*, *63*, 356–369. https://doi.org/10.1016/j.ijggc.2017.06.019

Falcon-Suarez, I., North, L., Amalokwu, K., & Best, A. (2016). Integrated geophysical and hydromechanical assessment for CO_2 storage: Shallow low permeable reservoir sandstones. *Geophysical Prospecting*, *64*(4), 828–847. http://doi.org/10.1111/1365-2478.12396

Falcon-Suarez, I., Papageorgiou, G., Chadwick, A., North, L., Best, A., & Chapman, M. (2018). CO_2-brine flow-through on an Utsira Sand core sample: Experimental and modelling. Implications for the Sleipner storage field. *International Journal of Greenhouse Gas Control*, *68*, 236–246. https://doi.org/10.1016/j.ijggc.2017.11.019

Falcon-Suarez, I. H., Amalokwu, K., Delgado-Martin, J., Callow, B., Robert, K., North, L., et al. (2019). Comparison of stress-dependent geophysical, hydraulic and mechanical properties of synthetic and natural sandstones for reservoir characterization and monitoring studies. *Geophysical Prospecting*, *67*(4), 784–803. https://doi.org/10.1111/1365-2478.12699

Fortin, J., Guéguen, Y., & Schubnel, A. (2007). Effects of pore collapse and grain crushing on ultrasonic velocities and V_p/V_s. *Journal of Geophysical Research*, *112*, B08207. https://doi.org/10.1029/2005JB004005

Gaus, I. (2010). Role and impact of CO_2-rock interactions during CO_2 storage in sedimentary rocks. *International Journal of Greenhouse Gas Control*, *4*(1), 73–89. http://doi.org/10.1016/j.ijggc.2009.09.015

Hangx, S., Bakker, E., Bertier, P., Nover, G., & Busch, A. (2015). Chemical–mechanical coupling observed for depleted oil reservoirs subjected to long-term CO_2-exposure—A case study of the Werkendam natural CO_2 analogue field. *Earth and Planetary Science Letters*, *428*, 230–242. http://doi.org/10.1016/j.epsl.2015.07.044

Hangx, S. J. T., Spiers, C. J., & Peach, C. J. (2010). Creep of simulated reservoir sands and coupled chemical-mechanical effects of CO_2 injection. *Journal of Geophysical Research*, *115*, B09205. http://doi.org/10.1029/2009JB006939

Iding, M., & Ringrose, P. (2010). Evaluating the impact of fractures on the performance of the In Salah CO_2 storage site. *International Journal of Greenhouse Gas Control*, *4*(2), 242–248. https://doi.org/10.1016/j.ijggc.2009.10.016

Jin, Z., Chapman, M., & Papageorgiou, G. (2018). Frequency-dependent anisotropy in a partially saturated fractured rock. *Geophysical Journal International*, *215*(3), 1985–1998. https://doi.org/10.1093/gji/ggy399

Knight, R., & Nolen-Hoeksema, R. (1990). A laboratory study of the dependence of elastic wave velocities on pore scale fluid distribution. *Geophysical Research Letters*, *17*(10), 1529–1532. https://doi.org/10.1029/GL017i010p01529

Kong, L., Gurevich, B., Zhang, Y., & Wang, Y. (2017). Effect of fracture fill on frequency-dependent anisotropy of fractured porous rocks. *Geophysical Prospecting*, *65*(6), 1649–1661. https://doi.org/10.1111/1365-2478.12505

Krevor, S., Blunt, M. J., Benson, S. M., Pentland, C. H., Reynolds, C., Al-Menhali, A., & Niu, B. (2015). Capillary trapping for geologic carbon dioxide storage—From pore scale physics to field scale implications. *International Journal of Greenhouse Gas Control*, *40*, 221–237. http://doi.org/10.1016/j.ijggc.2015.04.006

Lei, X., & Xue, Z. (2009). Ultrasonic velocity and attenuation during CO_2 injection into water-saturated porous sandstone: Measurements using difference seismic tomography. *Physics of the Earth and Planetary Interiors*, *176*(3:4), 224–234. https://doi.org/10.1016/j.pepi.2009.06.001

Mavko, G., Mukerji, T., & Dvorkin, J. (2009). *Rock physics handbook—Tools for seismic analysis in porous media*. New York: Cambridge University Press.

McCann, C., & Sothcott, J. (1992). Laboratory measurements of the seismic properties of sedimentary rocks. *Geological Society of London, Special Publication*, *65*(1), 285–297. https://doi.org/10.1144/gsl.sp.1992.065.01.22

Michael, K., Golab, A., Shulakova, V., Ennis-King, J., Allinson, G., Sharma, S., & Aiken, T. (2010). Geological storage of CO_2 in saline aquifers: A review of the experience from existing storage operations. *International Journal of Greenhouse Gas Control*, *4*(4), 659–667. http://doi.org/10.1016/j.ijggc.2009.12.011

Mikhaltsevitch, V., Lebedev, M., & Gurevich, B. (2014). Measurements of the elastic and anelastic properties of sandstone flooded with supercritical CO_2. *Geophysical Prospecting*, *62*(6), 1266–1277. https://doi.org/10.1111/1365-2478.12181

Muñoz-Ibáñez, A., Falcon-Suarez, I. H., Marín-Moreno, H., Martín, J. D., & Mackin, P. (2019). Transport properties of saline CO_2 storage reservoirs with unconnected fractures from brine-CO_2 flow-through tests. *Journal of Petroleum Science and Engineering*, *184*, 106551. https://doi.org/10.1016/j.petrol.2019.106551

Murphy, W. F. (1984). Acoustic measures of partial gas saturation in tight sandstones. *Journal of Geophysical Research*, *89*(B13), 11,549–11,559. https://doi.org/10.1029/JB089iB13p11549

Nakagawa, S., Kneafsey, T. J., Daley, T. M., Freifeld, B. M., & Rees, E. V. (2013). Laboratory seismic monitoring of supercritical CO_2 flooding in sandstone cores using the Split Hopkinson Resonant Bar technique with concurrent X-ray computed tomography imaging. *Geophysical Prospecting*, *61*(2), 254–269. https://doi.org/10.1111/1365-2478.12027

Nakatsuka, Y., Xue, Z., Garcia, H., & Matsuoka, T. (2010). Experimental study on CO_2 monitoring and quantification of stored CO_2 in saline formations using resistivity measurements. *International Journal of Greenhouse Gas Control*, *4*(2), 209–216. http://doi.org/10.1016/j.ijggc.2010.01.001

Nooraiepour, M., Bohloli, B., Park, J., Sauvin, G., Skurtveit, E., & Mondol, N. H. (2018). Effect of brine-CO_2 fracture flow on velocity and electrical resistivity of naturally fractured tight sandstones. *Geophysics*, *83*(1), WA37–WA48. https://doi.org/10.1190/geo2017-0077.1

North, L., Best, A. I., Sothcott, J., & MacGregor, L. (2013). Laboratory determination of the full electrical resistivity tensor of heterogeneous carbonate rocks at elevated pressures. *Geophysical Prospecting*, *61*(2), 458–470. https://doi.org/10.1111/j.1365-2478.2012.01113.x

Papageorgiou, G., & Chapman, M. (2017). Wave-propagation in rocks saturated by two immiscible fluids. *Geophysical Journal International*, *209*(3), 1761–1767. https://doi.org/10.1093/gji/ggx128

Papageorgiou, G., Falcon-Suarez, I., Chapman, M., & Best, A. (2018). Pressure-varying CO_2 distribution affects the ultrasonic velocities of synthetic sandstones. *International Journal of Greenhouse Gas Control*, *74*, 1–8. https://doi.org/10.1016/j.ijggc.2018.03.022

Rathore, J. S., Fjaer, E., Holt, R. M., & Renlie, L. (1995). *P*- and *S*-wave anisotropy of a synthetic sandstone with controlled crack geometry. *Geophysical Prospecting*, *43*(6), 711–728. https://doi.org/10.1111/j.1365-2478.1995.tb00276.x

Rutqvist, J. (2012). The geomechanics of CO_2 storage in deep sedimentary formations. *Geotechnical and Geological Engineering*, *30*(3), 525–551. http://doi.org/10.1007/s10706-011-9491-0

Suman, R. J., & Knight, R. J. (1997). Effects of pore structure and wettability on the electrical resistivity of partially saturated rocks—A network study. *Geophysics*, *62*(4), 1151–1162. https://doi.org/10.1190/1.1444216

Szewczyk, D., Holt, R. M., & Bauer, A. (2018). The impact of saturation on seismic dispersion in shales—Laboratory measurements. *Geophysics*, *83*(1), MR15–MR34. https://doi.org/10.1190/geo2017-0169.1

Tillotson, P., Chapman, M., Best, A. I., Sothcott, J., McCann, C., Shangxu, W., & Li, X.-Y. (2011). Observations of fluid-dependent shear-wave splitting in synthetic porous rocks with aligned penny-shaped fractures. *Geophysical Prospecting*, *59*(1), 111–119. https://doi.org/10.1111/j.1365-2478.2010.00903.x

Tillotson, P., Sothcott, J., Best, A. I., Chapman, M., & Li, X.-Y. (2012). Experimental verification of the fracture density and shear-wave splitting relationship using synthetic silica cemented sandstones with a controlled fracture geometry. *Geophysical Prospecting*, *60*(3), 516–525. https://doi.org/10.1111/j.1365-2478.2011.01021.x

Velcin, H., Dautriat, J., Sarout, J., Esteban, L., & Godel, B. (2020). Experimental reactivation of shear-fractured Berea and Boise sandstones by brine or liquid CO_2 injection at depth. *Journal of Geophysical Research: Solid Earth*, *125*, e2019JB018281. http://doi.org/10.1029/2019JB018281

Vialle, S., Contraires, S., Zinzsner, B., Clavaud, J.-B., Mahiouz, K., Zuddas, P., & Zamora, M. (2014). Percolation of CO_2-rich fluids in a limestone sample: Evolution of hydraulic, electrical, chemical, and structural properties. *Journal of Geophysical Research: Solid Earth*, *119*, 2828–2847. https://doi.org/10.1002/2013JB010656

Vialle, S., & Vanorio, T. (2011). Laboratory measurements of elastic properties of carbonate rocks during injection of reactive CO_2-saturated water. *Geophysical Research Letters*, *38*, L01302. http://doi.org/10.1029/2010GL045606

White, J. E. (1975). Computed seismic speeds and attenuation in rocks with partial gas saturation. *Geophysics*, *40*(2), 224–232. https://doi.org/10.1190/1.1440520

Winkler, K. W., & Plona, T. J. (1982). Technique for measuring ultrasonic velocity and attenuation spectra in rocks under pressure. *Journal of Geophysical Research*, *87*(B13), 10,776–10,780. https://doi.org/10.1029/JB087iB13p10776

Yin, C. S., Batzle, M. L., & Smith, B. J. (1992). Effects of partial liquid/gas saturation on extensional wave attenuation in Berea sandstone. *Geophysical Research Letters*, *19*(13), 1399–1402. https://doi.org/10.1029/92GL01159

Zhou, D., & Stenby, E. H. (1997). A percolation study of wettability effect on the electrical properties of reservior rocks. *Transport in Porous Media*, *29*(1), 85–98. https://doi.org/10.1023/A:1006598111378